Bulletin of the New Zealand Society for Earthquake Engineering, Vol. 51, No. 3, September 2018

SIMPLIFIED MOMENT-CURVATURE RELATIONSHIP IN ANALYTICAL FORM FOR CIRCULAR RC SECTIONS

Roberto Gentile[1], Francesco Porco[2], Domenico Raffaele[3] and Giuseppina Uva[4]

(Submitted *August 2017*; Reviewed *November 2017*; Accepted *January 2018*)

ABSTRACT

The behaviour of regular multi-span simply-supported bridges is strongly dependent on the behaviour of its piers. The response of a pier is governed, in general, by different mechanisms: flexure, shear, second order effects, lap-splice of longitudinal bars or their buckling. The flexural behaviour is an important part of the problem, and it can be characterised through the equivalent plastic hinge length and the Moment-Curvature law of the fixed end. In this paper, a procedure to calculate the Moment-Curvature relationship of circular RC sections is proposed which is based on defining the position of few characteristic points. The analytical formulation is based on adjusted polynomial functions fitted on a database of fibre-based analyses. The proposed solution is based on three parameters: dimensionless axial force, mechanical ratio of longitudinal reinforcement, geometrical ratio of transverse reinforcement. A benchmark case is presented to compare the solution to a FEM non-linear analysis. Even if it is based on few input data, this solution allows to have good indicators on the material performances (e.g. yielding, spalling, etc). For these reasons, the proposed approach is deemed to be particularly effective in performing quick yet accurate mechanics-based regional-scale assessment of bridges.

INTRODUCTION

The seismic vulnerability of existing structures has become a relevant theme in earthquake engineering, and great attention has been devoted to bridge structures, in order to perform vulnerability inventory at a regional scale. In fact, for example, most of the Italian RC bridges were built around the 1960s referring to codes with no "anti-seismic philosophy". Moreover, a bridge can often be a crucial node of a transport web and thus its performance should be guaranteed even in the aftermath of an earthquake. Hence, having an inventory of the structural performances of the bridges in a region is crucial in order to plan mitigation actions. This might be also needed to quickly assess a large group of damaged bridges in the aftermath of an earthquake. The 2016 Kaikoura Earthquake is a clear example of this situation [1].

Considering the large amount of structures involved and the shortage of resources, it is cost-ineffective to perform detailed structural analyses (e.g. non-linear analyses) for the whole portfolio [2]. Therefore, a multi-level approach is usually preferred, by starting from a large-scale analysis at the regional level, in which a first screening and prioritisation is performed by using poor data and simplified models. In the successive stages, the accuracy and detail of the assessment is progressively refined for specific subsets of elements at risk.

Traditionally, regional-scale analysis resorts to typological or semi-empirical vulnerability methods that involve the use of calibrated indexes, e.g. [3]. As a possible approach to manage the regional scale, some researchers have proposed the definition of simplified capacity curves for typological classes fitted on detailed nonlinear analyses for a representative number of "ideal" sample case studies [4]. Alternatively, other classes of simplified methods allow to assess the performance of relatively regular bridges based on a rational mechanical approach, although under simplified assumptions. Provided that the deck remains elastic and the bearings do not fail, the energy dissipation capacity of a bridge is concentrated in the piers [5]. Therefore, the vulnerability of the whole structure can be expressed by studying the capacity curves of the piers, modelled as equivalent SDOF systems, in the transverse and in the longitudinal direction. In this last case, each pier can still be considered as an independent oscillator by considering the "effective" mass pertaining to the adjacent spans. Depending on the direction of the analysis, it is therefore necessary to consider two distinct simplified models characterised by different parameters [6-8]. Based on the fixity condition of the piers, an appropriate shear span length can be defined, and the Force-Displacement flexural behaviour is defined by the Moment-Curvature relationship of a critical section. For simply supported bridges, the critical section is located at the base. For a detailed analysis of a single bridge, Moment-Curvature is typically calculated with a software (e.g. KSU_RC [9], Cumbia [10], etc). The flexural capacity curve can be possibly modified by the occurrence of additional failure mechanisms such as shear, longitudinal bars buckling, lap-slice, second order effects.

In view of a regional-scale analysis for a large portfolio of bridges and of the derivation of probabilistic fragility curves [11-13], it is particularly desirable to have a rapid yet accurate formulation of the Moment-Curvature relationship, which is the specific objective of this paper (Figure 1). In particular, in this study it is proposed a polynomial analytic solution fitted against an extensive dataset of sectional analyses that guarantees an accurate, rapid and computationally inexpensive flexural characterisation of the sections of the piers. Alternatively, for a

[1] *Corresponding Author, Ph.D. candidate, Dpt. of Civil, Environmental, Land, Building Engineering and Chemistry, Polytechnic University of Bari, Bari, Italy, roberto.gentile@poliba.it*

[2] *Lecturer, Dpt. of Civil, Environmental, Land, Building Engineering and Chemistry, Polytechnic University of Bari, Bari, Italy, francesco.porco@poliba.it*

[3] *Senior Lecturer, Dpt. of Civil, Environmental, Land, Building Engineering and Chemistry, Polytechnic University of Bari, Bari, Italy, domenico.raffaele@poliba.it*

[4] *Associate Professor, Dpt. of Civil, Environmental, Land, Building Engineering and Chemistry, Polytechnic University of Bari, Bari, Italy, giuseppina.uva@poliba.it*

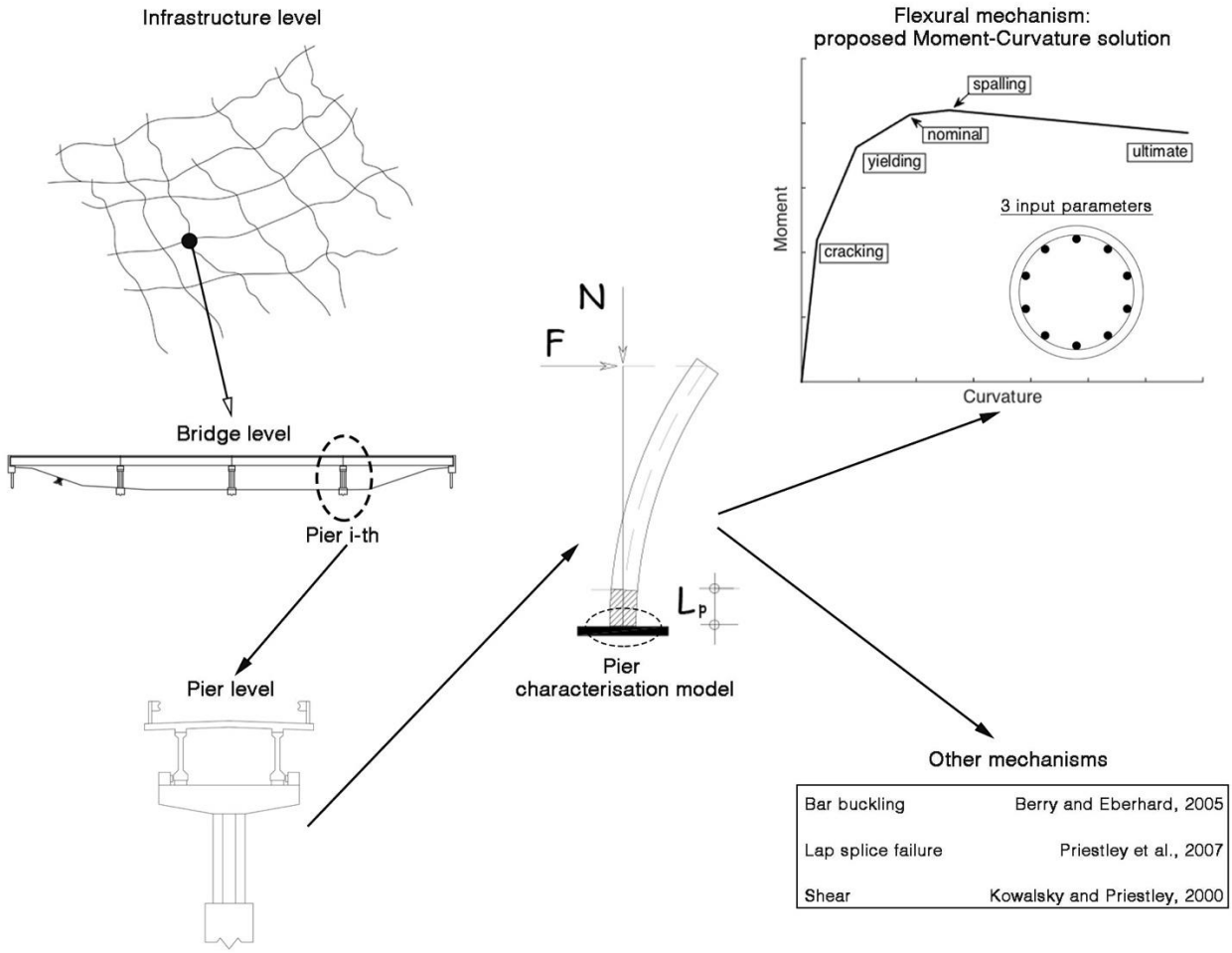

Figure 1: Regional-scale seismic vulnerability of bridges.

detailed assessment, such a rapid formulation can be used to verify and validate the results of the numerical Moment-Curvature analyses. Once the simplified Moment-Curvature is calculated, the aforementioned additional mechanisms can be easily introduced in the model by using acknowledged literature studies (shear failure [14], longitudinal bars buckling [15], lap-splice [16], second order effects [17]).

In the paper, the solution for circular sections is presented, but it can be generalised to other section shapes, which are currently being studied.

METHODOLOGY FOR DERIVING THE ANALYTICAL SIMPLIFIED $M-\varphi$ FORMULATION

The Moment-Curvature $(M-\varphi)$ relationship of RC circular sections is calculated by defining the position of few characteristic points. Each of these is defined in analytical form depending on 3 parameters (also used in other literature studies, e.g. [18, 19]): dimensionless axial force, mechanical ratio of longitudinal reinforcement, volumetric ratio of transverse reinforcement. To do so, a database of Moment-Curvature diagrams was created conducting fibre-based analyses (from now on referred to as "exact" numerical solution). The numerical analyses were carried out using the software by Esmaeily and Peterman [9]. The results were processed using MATLAB in order to define the characteristic points of each $(M-\varphi)$ curve. Finally, based on least squares method linear regression, a polynomial relation was calculated for each characteristic moment or curvature (from now on referred to as simplified analytical solution). The approach herein proposed is based on realistic stress-strain relationships for concrete and steel and for this reason the results are particularly accurate. The reliability of the proposed solution is proved analysing a numerical case study pier and comparing the results with a FEM non-linear analysis, showing good agreement.

Definition of the Characteristic Points

Each software-based $(M-\varphi)$ curve was analysed with a MATLAB function specifically designed for this study. Having as input the Moment-Curvature law in tabular form, the function extracts 7 characteristic points corresponding to different limit states of the section (see Figure 2). Based on these points, a multi-linear approximation of the $(M-\varphi)$ curve can be obtained (an example is given in Figure 3).

The chosen characteristic points are:

Cracking: For the cracking point, a strain of ε_{ct} is measured in the furthermost concrete fibre in the section (see Figure 2). More specifically, this is the point for which Eq. 1 is satisfied. In this equation, D is the diameter of the cross-section, $n.a.$ is the neutral axis depth, c is the clear cover, f_{ct} is the concrete flexure tensile strength (Eq. 6), ε_c is the strain in the furthermost compressed concrete core fibre;

$$\frac{D-n.a.}{n.a.-c}\varepsilon_c = \varepsilon_{ct} \quad where \quad \varepsilon_{ct} = \frac{f_{ct}}{E_c} \tag{1}$$

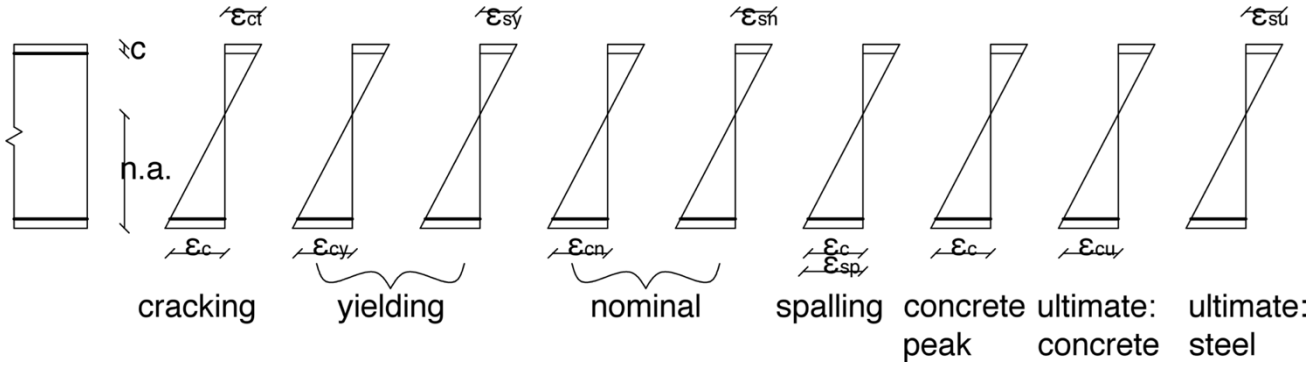

Figure 2: Strain state of the section in the characteristic points.

Concrete Yielding: Defined as the point on the $(M-\varphi)$ curve that corresponds to a strain of $\varepsilon_{cy}=0.002$ in the extreme core concrete fibre in compression.

First Yield: The minimum value between concrete yielding and the point on the $(M-\varphi)$ curve that corresponds to the first tension yielding of the reinforcement bar furthest from the neutral axis [17];

Nominal: This points corresponds to a compressive strain of $\varepsilon_c=0.004$ in the extreme core concrete compression fibre or $\varepsilon_s=0.015$ in the furthermost tension rebar, whichever occurs first [17];

Spalling: The point on the $(M-\varphi)$ response for which the spalling strain $\varepsilon_{sp}=0.0045$ is induced in the extreme fibre of the cover concrete (Figure 2) according to Eq. 2;

$$\frac{n.a.}{n.a.-c}\varepsilon_c=\varepsilon_{sp} \tag{2}$$

Peak of Confined Concrete: This point represents the curvature that induces a strain, in the extreme core concrete fibre, equal to its strain at peak stress in the stress-strain relationship (Figure 5). This point can be used to understand the starting of the softening of the concrete;

Ultimate: The last point of the $(M-\varphi)$ curve. The failure of the section can be due to the achievement of the ultimate compressive strain in confined concrete or strain at ultimate stress in the extreme tension rebar.

The transformation in dimensionless form $(m-\chi)$ is done with Equations 3 and 4, in which R is the radius of the cross-section and f_c is the unconfined concrete strength.

$$m=\frac{M}{\pi R^3 f_c} \tag{3}$$

$$\chi=\varphi R \tag{4}$$

CONSTRUCTION OF THE DATABASE

Basic Parameters

The parameters involved in the definition of the flexural behaviour of RC circular sections are several: radius R, clear cover c, axial force N, compression strength of concrete in unconfined conditions f_c, tension strength of concrete f_{ct}, concrete modulus of elasticity E_c, yielding strength of longitudinal and transverse reinforcement f_{ys}, f_{yh}, moduli of elasticity of the steel E_s, E_h, number and diameter of longitudinal reinforcement bars n_l, d_l, diameter and spacing of transverse reinforcement d_h, s.

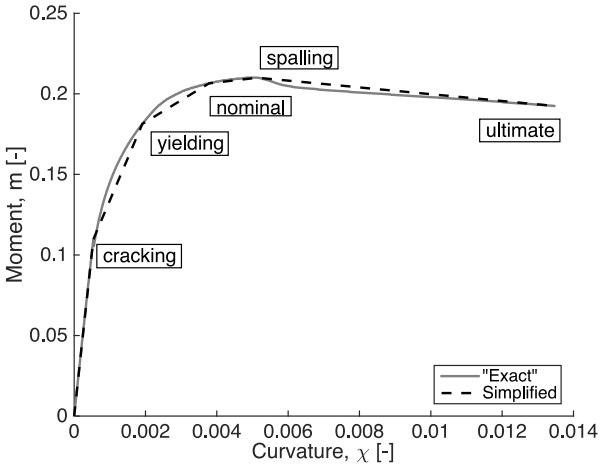

Figure 3: Simplified Moment-Curvature relationship.

It is clear that, for the purpose of this work, it is inconvenient to have such a large number of parameters and, for this reason, some assumptions were adopted:

- concrete tensile strength f_t (for uniform tensile stress) was related to its compression strength (f_c) according to Eq. 5, provided in the Italian code [21]. Moreover, Eq. 6 was used in order to consider the tensile strength appropriate for flexure actions (f_{ct}). This choice is not likely to limit the field of application of the final formulations, since it only affects the cracking point of the Moment-Curvature law;

$$f_t=0.3f_c^{2/3} \tag{5}$$

$$f_{ct}=1.2f_t \tag{6}$$

- longitudinal and transverse reinforcement steel have the same yield stress (f_{ys}, f_{yh} respectively) and elastic modulus (E_s, E_h respectively), according to Eq. 7;

$$f_{yh}=f_{ys} \quad and \quad E_h=E_s \tag{7}$$

- longitudinal reinforcement is composed by n_l evenly distributed bars of equal diameter d_l. The total area of longitudinal steel is defined with Eq. 8;

$$A_s=\frac{n_l(\pi d_l^2)}{4} \tag{8}$$

- the clear cover, c, is proportional to the radius of the section according to Eq. 9;

$$c = 0.05R \tag{9}$$

- the diameter is fixed to $1m$. This was done considering that the relationship between a given limit state curvature and the diameter of the section is linear (see, for example [17], in which this is shown for yielding and ultimate curvature).

The remaining parameters of the problem were grouped into 3 dimensionless parameters based on dimensional analysis (axial force ratio υ, mechanical ratio of longitudinal reinforcement ω, volumetric ratio of transverse reinforcement ρ_{sp}) so that a given circular RC section can be completely defined by them.

The idea is that a variation in υ (Eq. 10) can be interpreted as a variation in the normal force N, the concrete compression strength f_c or the radius R. An analogous idea applies for Equations 11 and 12.

$$\upsilon = \frac{N}{\pi f_c R^2} \tag{10}$$

$$\omega = \frac{A_s f_y}{\pi f_c R^2} \tag{11}$$

$$\rho_{sp} = \frac{4A_{sp}}{(2R - 2c)s} \tag{12}$$

Range of the Parameters

The discrete values of the basic parameters used to construct the database are listed in Table 1. It is clear that some of the studied values are greater than the maximum expected ones for real existing bridge piers. Those were added to the database for the sake of completeness, and to study the trends of the characteristic points of the $(M - \varphi)$ curve.

Table 1: Range of the parameters.

Parameter	Values
υ	0, 0.1, 0.2, 0.3, 0.4, 0.5, 0.6, 0.7, 0.8, 0.9, 1
ω	0.05, 0.1, 0.2, 0.4, 0.6, 0.8
ρ_{sp}	0, 0.001, 0.002, 0.004, 0.006, 0.008, 0.01

For the analyses in the database, the values $R = 1m$ and $f_c = 31.83MPa$ were fixed and the value of N corresponding to υ was calculated according to Eq. 10. Analogously, $f_y = 450MPa$ and $n_l = 22$ were fixed so the cross-sectional area of a single rebar was calculated using Equations 11 and 8. It is worth mentioning that since the relationship between steel yield stress and strength of the cross-section can be assumed to be linear [17], this choice is unlikely to limit the scope of the simplified formulations proposed in this paper.

Fixing the clear cover (Eq. 9), the spacing of the stirrups ($s = 0.1m$), and the other above-mentioned values, the cross-sectional area of the stirrup was calculated using Eq. 12.

Execution of the Analyses

Based on the chosen discrete values of the input parameters, a *Moment-Curvature* analysis was conducted for each combination of them (11x6x7=462 combinations). The analyses were carried out with the software KSU-RC [9]. The fibre discretisation of the cross-section adopted in the analyses is shown in Figure 4.

The relationship proposed in Mander et al., 1988 [20] was used for concrete, considering the confined and unconfined behaviour (Figure 5). It is worth mentioning that confined concrete ultimate strain was limited to 0.02 when the calculation according to reference [20] yielded higher values.

The behaviour of steel was modelled with the stress-strain relationship shown in Figure 6, proposed in Reference [9]. The curve is linear up to yielding, with a plateau up to a strain of K_1 times the yielding strain and followed by a parabolic shape. The peak corresponds to a strain of K_2 times the yielding strain and a strain of K_3 times the yielding strain corresponds to the ultimate strain point at rupture. K_4 is the tensile strength to yield stress ratio. These parameters were fine-tuned to be representative of a commercial steel with a nominal yield stress ranging between 400 and 500 MPa (e.g. the Italian B450C [21] and the New Zealand grade 500 [22, 23]). $K_1 = 10$ was used to model the length of the yield plateau. Recent research [24] corroborates this choice. The remaining parameters are: $K_2 = 30$, $K_3 = 55, K_4 = 1.3$. It is worth mentioning that 0.06 was adopted as steel ultimate strain, to implicitly consider low cycle fatigue failure, as suggested in the 2017 New Zealand guidelines for seismic assessment [22]. Figure 6 shows that, with these assumptions, the adopted stress-strain relationship is in close agreement with the widely utilised curve proposed in King et al., 1986 [25]. This is deemed to indirectly demonstrate the suitability of the adopted stress-strain curve.

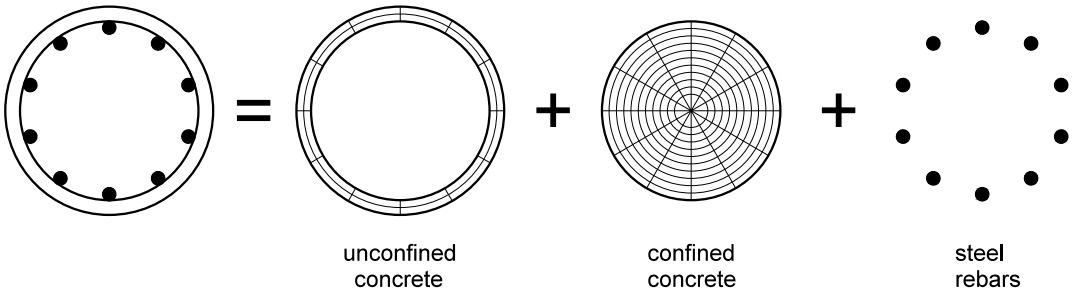

Figure 4: Cross-section fibre model.

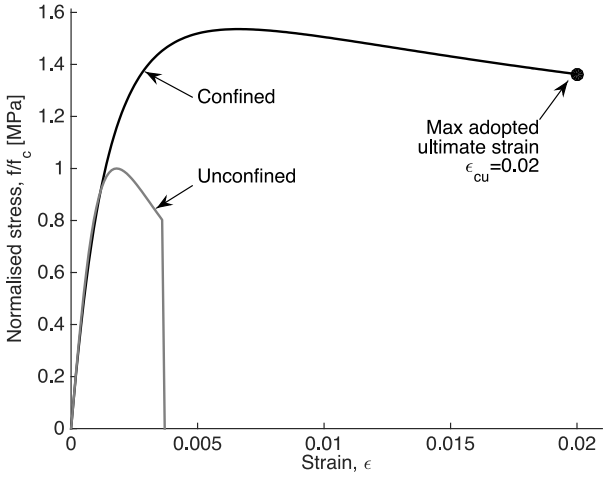

Figure 5: Concrete stress-strain relationship.

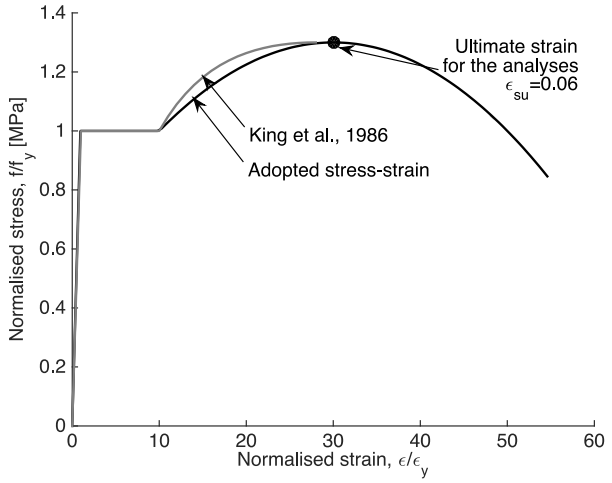

Figure 6: Steel stress-strain relationship

POST PROCESSING

A study was conducted to investigate the variability of the characteristic moments and curvatures with respect to the fundamental parameters chosen. In Figure 7, the trend of the most meaningful characteristic points is represented as a function of the dimensionless axial force, υ, and a fixed value of both longitudinal (ω) and transverse reinforcement (ρ_{sp}) ratios. In Appendix **A** some more synthetic plots are represented that account for the variability of the parameters ω and ρ_{sp}. In such plots (Figure 13 to Figure 18), the mechanical ratio of the longitudinal reinforcement, ω, is fixed, each characteristic point has a different line colour (e.g. green is for yielding), and the line width increases with the increase of the volumetric ratio of transverse reinforcement (the dashed line is for unconfined).

CURVE FITTING

By knowing the values of the characteristic moments and curvatures for each case in the database, 14 polynomials in three variables (axial load ratio, mechanical ratio of longitudinal reinforcement, volumetric ratio of transverse reinforcement) were calibrated to fit the data based on a least square method linear regression. It is noteworthy that the cases in which $\rho_{sp} = 0$ were studied only for control purposes and so they were excluded from the fitting. For the same reason, the cases with $\upsilon = 0.9$ and $\upsilon = 1$ were excluded too. It is worth mentioning that the results of the parametric analysis, Figure 13 to Figure 18, can be adopted to manually construct "by-hand" the capacity curve of a given RC circular section. Nonetheless, it is deemed that the adjusted polynomial functions are more effective if a great number of applications is needed, since they can be easily implemented in a spreadsheet or a computer routine.

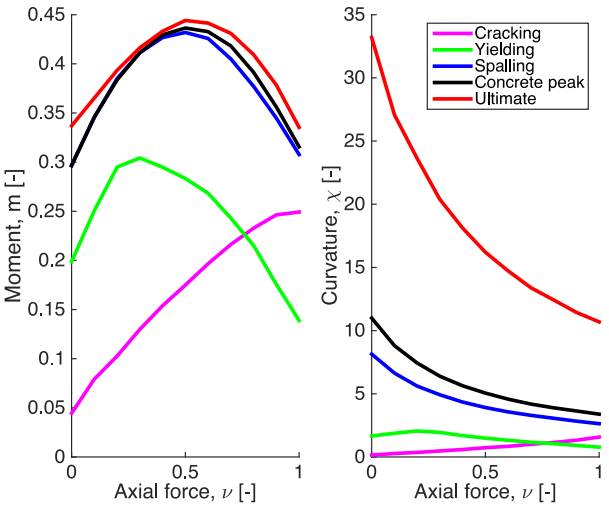

Figure 7: Trend of the characteristic moments and curvatures for $\omega = 0.4$ and $\rho_{sp} = 0.006$.

The degree of the polynomials in each of the three variables was chosen based on the trends represented in Figure 13 to Figure 18. The coefficients of the fitting were defined in such a way that a p-value smaller than 5% was obtained for all of them. Although this is not a statistical study, it is worth mentioning that the adjusted R-squared parameter is 0.99 for the moment polynomials and ranges between 0.90 and 0.99 for the curvature ones. The structure of the polynomials is described in Equations 13 and 14, while the a_i coefficients for each function are given in Table 5 and Table 6, in Appendix **A**.

$$\begin{aligned}\chi_{char} = {} & a_0 + a_1\upsilon + a_2\omega + a_3\rho_{sp} + a_4\upsilon^2 + a_5\upsilon\omega \\ & + a_6\omega^2 + a_7\upsilon\rho_{sp} + a_8\omega\rho_{sp} \\ & + a_9\upsilon^3 + a_{10}\upsilon^2\omega + a_{11}\upsilon\omega^2 \\ & + a_{12}\upsilon^2\rho_{sp} + a_{13}\upsilon\omega\rho_{sp} \\ & + a_{14}\omega^2\rho_{sp}.\end{aligned} \tag{13}$$

$$\begin{aligned}m_{char} = {} & a_0 + a_1\upsilon + a_2\omega + a_3\rho_{sp} + a_4\upsilon^2 + a_5\upsilon\omega \\ & + a_6\omega^2 + a_7\upsilon\rho_{sp} + a_8\omega\rho_{sp} \\ & + a_9\upsilon^3 + a_{10}\upsilon^2\omega + a_{11}\upsilon\omega^2 \\ & + a_{12}\upsilon^2\rho_{sp} + a_{13}\upsilon\omega\rho_{sp} \\ & + a_{14}\omega^2\rho_{sp} + a_{15}\rho_{sp}^2.\end{aligned} \tag{14}$$

ULTIMATE CURVATURE CORRECTION FACTOR

Concrete compressive strength was not explicitly considered as an input value for the database, since the analyses were conducted assuming $f_c = 31.83MPa$. According to the energy-based assumptions in Mander's model, the ultimate strain of confined concrete depends on the compressive strength of unconfined concrete. In particular, fixing the ratio of transverse reinforcement, the greater the compressive strength the less the ultimate strain of confined concrete. For a given value of ρ_{sp}, the relationship between ultimate strain of confined concrete and strength of unconfined concrete is parabolic (as shown in Figure 8). A similar pattern is to be expected for the ultimate curvature, strongly correlated to concrete ultimate strain.

To capture this trend, a sensitivity analysis with respect to f_c was carried out and a correction factor for the ultimate curvature polynomial was calculated. A group of RC sections was defined

with different values of f_c but equal value of the parameters υ, ω and ρ_{sp} (Eqs. 10, 11 and 12). For each of them, a *Moment-Curvature* analysis and a post-processing were conducted, calculating the ultimate dimensionless curvature $\chi_u(f_c)$. The same values, named $\chi_u(31.83)$, were predicted with the ultimate curvature polynomial. The ratios of the above-mentioned parameters were used to fit the 2nd-order polynomial "Correction Factor (CF)", shown in Eq. 15. This allows to take into account the appropriate value of the concrete strength and correct the ultimate curvature prediction according to Eq. 16. Basically, the ultimate curvature is calculated multiplying the value predicted according to the ultimate curvature polynomial (depending on υ, ω, ρ_{sp}) to correction factor (which depends on f_c).

$$CF = \frac{\chi_u(f_c)}{\chi_u(31.83)} = \\ = 0.000738 f_c^2 - 0.078268 f_c + 2.747041 \quad (15)$$

$$\chi_u(f_c) = CF\,\chi_u(31.83) \quad (16)$$

Figure 9 shows, respectively for $f_c = 20MPa$ and $f_c = 50MPa$, the comparison of the "exact" $(M-\varphi)$ diagram (dash-dot line), the simplified one with (solid line) or without (dashed line) using the correction factor. It is clear that using the "non-corrected" polynomial, the ultimate curvature is under-predicted for $f_c = 20MPa$ and over-predicted for $f_c = 50MPa$. The "corrected" version leads to a very good match with the "exact" solution in terms of ultimate curvature.

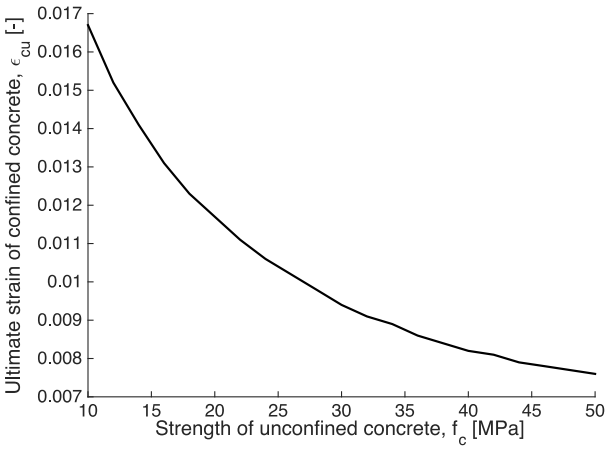

Figure 8: Ultimate strain of confined concrete with respect to the unconfined concrete strength for an equal value of volumetric ratio of transverse reinforcement.

ACCURACY OF THE FUNCTIONS

The polynomials that allow the construction of the $(M-\varphi)$ curve were tested with the procedure that follows. A group of 10 RC circular sections was defined with random yet plausible values of the input parameters (shown in Table 7, in Appendix A). Each "test case" was analysed (with the same procedure used for the database) to obtain the characteristic moments and curvatures. Then the polynomials herein proposed were used to predict the same values (the ultimate curvature was multiplied by the correction factor).

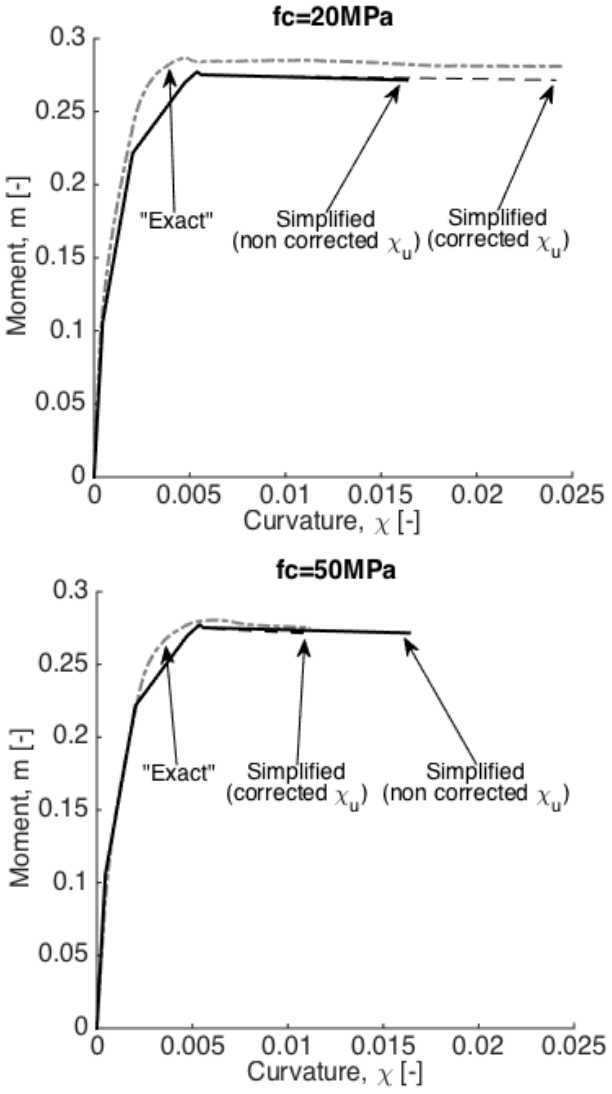

Figure 9: Role of the ultimate curvature correction factor.

According to Eq. 17, the error (ERR) of each prediction was calculated and a global error (ERR_{glob}) was defined by Eq. 18 (shown in Table 2). For the characteristic moments, an under prediction lower than 11% is registered, except for the ultimate moment (15.9%). On the other hand, more scatter is registered for the characteristic curvatures, with a considerably smaller absolute error. These trends are shown in detail in Figure 10 through predicted vs measured plots, comprehensive of the full dataset used for the curve fitting. This gives a complete overview of the accuracy of the proposed model.

$$Err = 100\left|\frac{measured - predicted}{measured}\right| [\%] \quad (17)$$

$$Err_{glob} = \frac{\sum_{i=1}^{10} Err_i}{10} [\%] \quad (18)$$

NUMERICAL APPLICATION

The aim of this section is to demonstrate that the proposed simplified procedure to evaluate the *Moment-Curvature* diagram of an RC cross-section is a reliable input for the assessment of the performance of a bridge pier. Therefore, a numerical validation of the above-mentioned procedure is presented herein. It is assumed that the geometric and

Table 2: Global error [%] of the functions, related to 10 Test sections.

	χ_{CR}	χ_{Yc}	χ_{Y}	χ_{P}	χ_{N}	χ_{SP}	χ_{U}	m_{CR}	m_{Yc}	m_{Y}	m_{P}	m_{N}	m_{SP}	m_{U}
ERR_{glob}	10.1	10.4	6.6	11.9	5.7	5.6	4.9	6.0	10.7	11.1	7.1	4.2	3.9	15.9

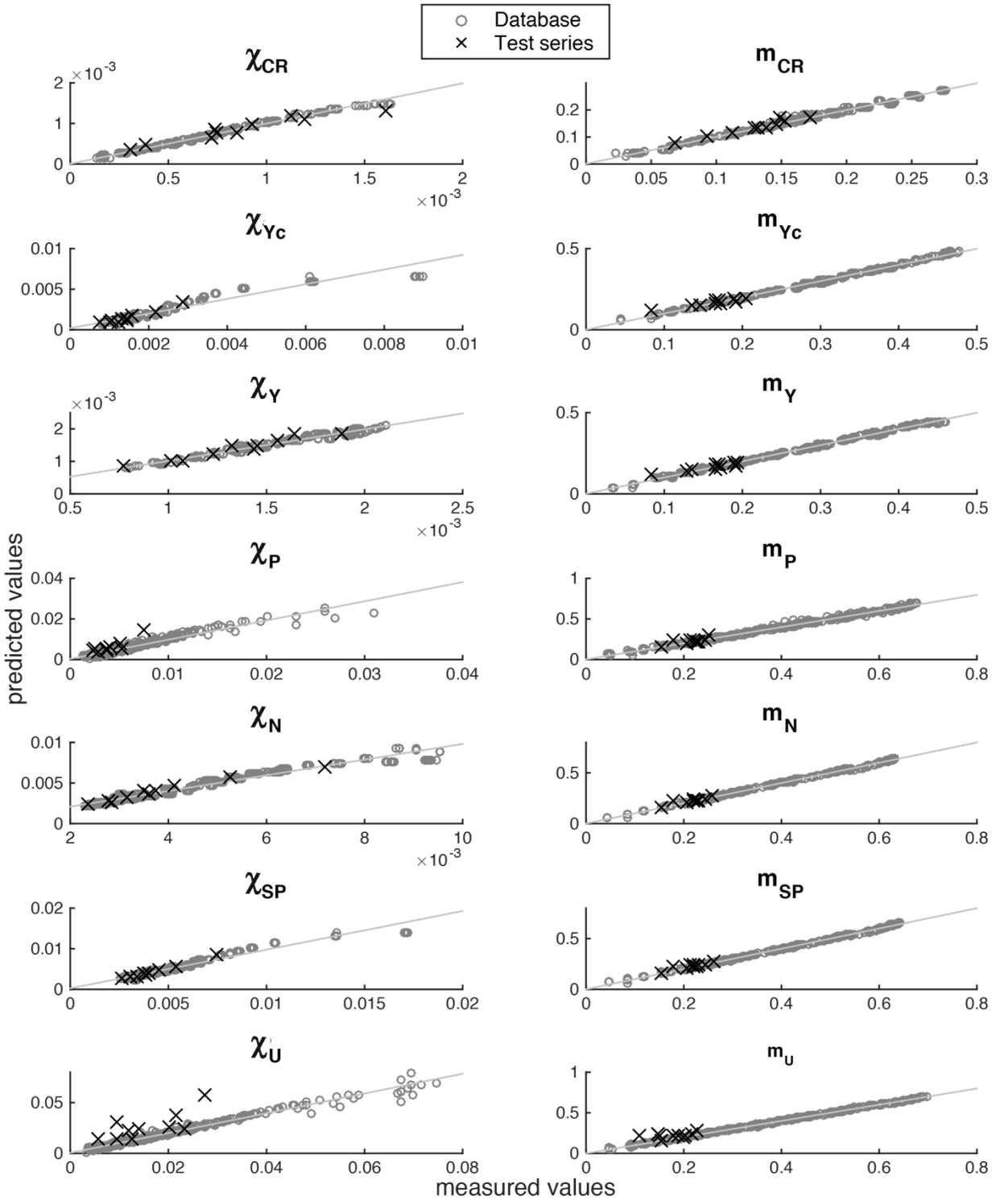

Figure 10: Predicted vs measured plots.

mechanical parameters of an ideal bridge pier, belonging to a simply-supported bridge, are the ones listed in Table 3

It is worth noting that the behaviour of the pier depends on the presence of seismic restraints and this can be taken into account in a simplified way by considering the effective mass pertaining to the pier itself [6]. For this reason, it is necessary to conduct two separate analyses, one for the transverse and one for the longitudinal direction, varying the axial force on the pier.

The flexural behaviour of the base section of the pier was predicted using the characteristic polynomials (Equations 13 and 14) and transformed in dimensional form according to Equations 3 and 4. The *Force-Displacement* $(F-\delta)$ was calculated according to Equations 19 and 20, in which φ is the curvature, φ_Y is the yield curvature, M is the moment, L is the length of the pier and L_p $(=0.64m)$ is the plastic hinge length, calculated according to Priestley and Park, 1987 [26].

This curve might be "corrected" in order to take into account the different mechanisms, but the benchmark case was chosen in such a way that the collapse was only governed by axial force and bending: therefore, no additional action was needed. In Figure 11, the simplified $(M-\varphi)$ diagrams are compared to the "exact" numerical sectional analysis, carried out with KSU_RC [9], SAP2000 [27] and Cumbia [10]. A very good match is registered, with a modest overestimation of the moment in the post-yielding branch (numerical values are discussed below).

$$\delta = \begin{cases} \dfrac{\varphi L^2}{3} & if\ \varphi \le \varphi_Y \\ \dfrac{\varphi_Y L^2}{3} + (\varphi - \varphi_Y) L_p \left(L - 0.5 L_p\right) & if\ \varphi > \varphi_Y \end{cases} \quad (19)$$

$$F = \frac{M}{L} \quad (20)$$

The pier was also modelled by means of 12 “beam” elements using the FEM software *SAP2000 V18* [27]. Using the "Fiber P M2 M3 hinge", the cross-section was discretised into 600 fibres assigning the same constitutive laws used in the database. The pier was studied through a displacement-control Pushover analysis under a horizontal force applied to the tip of it. The obtained capacity curve is compared to the one calculated according to Eq. 19 (Figure 12). The results obtained with the simplified procedure are particularly close to the “exact” FEM solution, reflecting the trends registered for the Moment-Curvature. This is confirmed in Table 4, which shows the analytical-to-numerical errors, calculated for force and displacement at the peak of the curve (δ_{peak}, F_{peak}) and at the ultimate condition (δ_u, F_u).

Table 3: Geometric and mechanical properties of the example pier.

	L	D	c	n_l	d_l	d_h	s	f_c	f_{ys}	N	ν	ω	ρ_{sp}
	(m)	(m)	(m)	(-)	(mm)	(-)	(mm)	(MPa)	(MPa)	(MN)	(-)	(-)	(-)
Transverse	6	2	0.05	30	26	16	70	20	450	13.87	0.221	0.114	0.006
Longitudinal	6	2	0.05	30	26	16	70	20	450	17.85	0.284	0.114	0.006

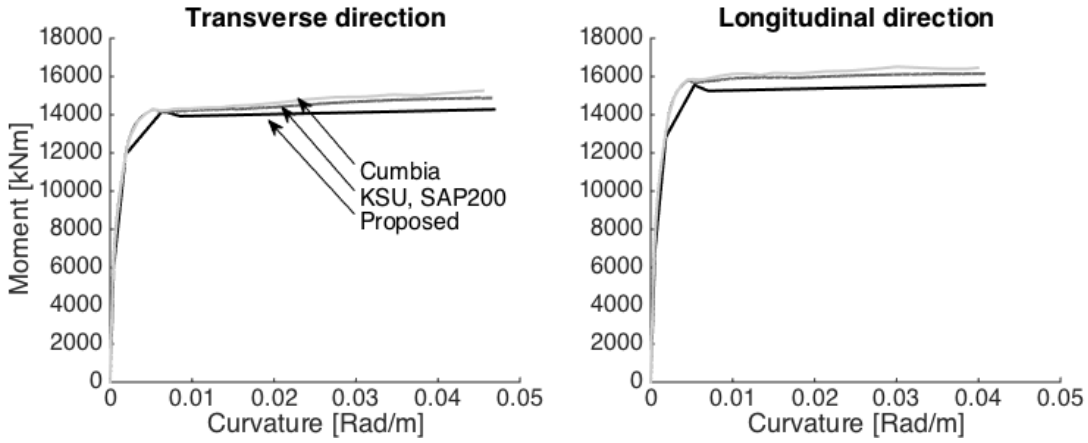

Figure 11: Moment-Curvature: comparison between "exact" and simplified procedure, transverse and longitudinal direction.

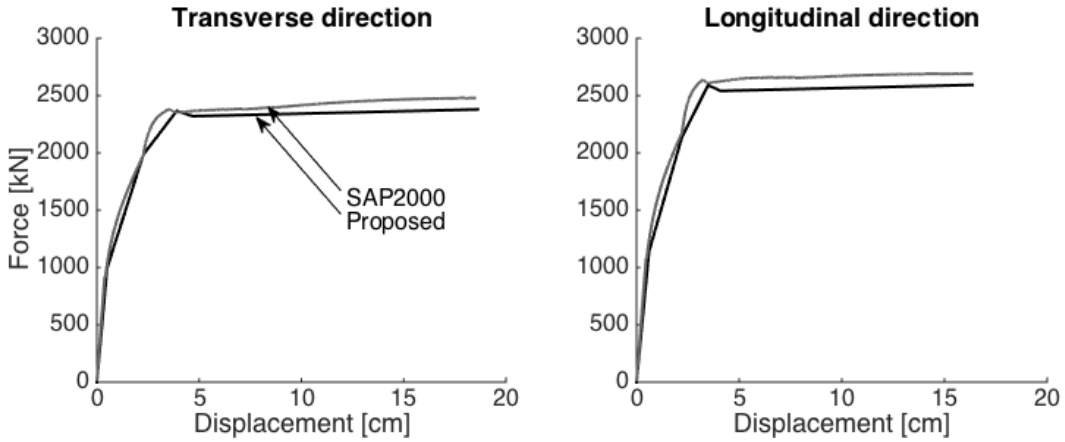

Figure 12: Comparison of the pier capacity curves, transverse and longitudinal directions.

Table 4: Simplified vs refined FEM analyses: numerical comparison of the results.

	d_{peak}	F_{peak}	d_u	F_u
Transverse	11.43%	-0.55%	0.43%	-4.03%
Longitudinal	10.48%	-1.41%	-0.18%	-3.64%

CONCLUSIONS AND FURTHER DEVELOPMENTS

This paper deals with the development of a polynomial solution for the characterisation of the flexural behaviour of RC circular bridge piers. In particular, it is proposed to calculate the *Moment-Curvature* relationship of RC circular sections by defining the position of few characteristic points. Each of these is defined in analytical form depending on 3 parameters: dimensionless axial force, mechanical ratio of longitudinal reinforcement, volumetric ratio of transverse reinforcement. The solution is based on polynomial functions fitted against a large database of fibre-based numerical *Moment-Curvature* diagrams. The proposed procedure was compared to a refined non-linear FEM model showing good match.

The polynomial formulation is particularly effective within the framework of the regional seismic assessment of RC bridges, in order to perform a large number of analyses and derive probabilistic fragility curves. The use of such a mechanically-based method, instead of commonly-used empirical methods based on calibrated indices, guarantees much more accuracy and management of uncertainty. On the other hand, the intrinsic simplicity of the proposed solution allows to perform the required large number of analyses with a negligible computational effort. The formulation is well suited for the implementation within computer-based automatic procedures. Other significant section shapes are currently being analysed, in order to provide a more flexible and general assessment tool.

ACKNOWLEDGMENTS

The research presented in this paper was partially funded by the Project ReLUIS-DPC 2014-2018, "Linea C.A." – R.U. Politecnico di Bari (G.Uva) and the FRA 2012 project (Politecnico di Bari, D.Raffaele).

REFERENCES

1 Palermo A, Liu R, Rais A, McHaffie B, Andisheh K, Pampanin S, Gentile R, Nuzzo I, Graniero M, Loporcaro G, McGann C and Wotherspoon L (2017). "Performance of road bridges during the 14th November 2016 Kaikoura earthquake". *Bulletin of the New Zealand Society for Earthquake Engineering*, **50**(2): 253-270.

2 Pinho R, Monteiro R, Casarotti C and Delgado R (2009). "Assessment of Continuous Span Bridges through Nonlinear Static Procedures". *Earthquake Spectra*, **25**(1): 143–159.

3 Kircher CA, Whitman RV and Holmes WT (2006). "HAZUS Earthquake Loss Estimation Methods". *Natural Hazard Review*, **7**:45-59.

4 Broglio S, Crowley H and Pinho R (2010). "Simplified Capacity Curves for RC Bridges". *Proceedings of 14th European Conference on Earthquake Engineering*, Ohrid, Republic of Macedonia, 30/08/2010-03/09/2010.

5 Fardis MN (2007). "*Risk Mitigation for Earthquakes and Landslides. Guidelines for Displacement-Based Design of Buildings and Bridges*". Report No. 5/2007, IUSS Press, Pavia, Italy.

6 Raffaele D, Porco F, Fiore A and Uva G (2014). "Simplified vulnerability assessment of reinforced concrete circular piers in multi-span simply supported bridges". *Structure and Infrastructure Engineering*, **10**(8): 950–962.

7 Raffaele D, Porco F, Uva G and Fiore A (2014). "Simplified assessment of seismic retrofitting interventions on RC circular piers in multi-span simply sup- ported bridges". *Proceedings of the 7th International Conference on Bridge Maintenance, Safety and Management*, Shanghai, China, 07-11/07/14. 2245–2252.

8 Raffaele D, Uva G, Porco F and Fiore A (2014). "About of seismic capacity of bridge piers: A simplified approach". *Proceedings of the 7th International Conference on Bridge Maintenance, Safety and Management*, Shanghai, China, 07-11/07/14. 2245–2252.

9 Esmaeily A and Peterman RJ (2007). "Performance analysis tool for reinforced concrete members". *Computers and Concrete*, **4**(5): 331–346.

10 Montejo LA and Kowalsky MJ (2007). "*Set of Codes for the Analysis of Reinforced Concrete Members"*. Technical Report No. IS-07-01, North Carolina State University, USA.

11 Padgett JE, Nielson BG and Desroches R (2008). "Selection of optimal intensity measures in probabilistic seismic demand models of highway bridge portfolios". *Earthquake Engineering and Structural Dynamics*, **37**: 711–725.

12 Zelaschi C, Monteiro R and Pinho R (2015). "Improved fragility functions for RC bridge populations". *Proceedings of the 5th ECCOMAS Thematic Conference on Computational Methods in Structural Dynamics and Earthquake Engineering*, Crete Island, Greece, 25-27 May 2015.

13 Miano A, Fatemeh J, De Risi R, Prota A and Manfredi G (2015). "A Case-Study on scenario-based probabilistic seismic loss assessment for a portfolio of bridges". *Proceedings of the 12th International Conference on Applications of Statistics and Probability in Civil Engineering, ICASP12*, Vancouver, Canada, 12-15/07/2015.

14 Kowalsky MJ and Priestley MJN (2000). "Improved Analytical Model for Shear Strength of Circular Reinforced Concrete Columns in Seismic Regions". *ACI Structural Journal*, 97-S42: 388-396.

15 Berry MP and Eberhard MO (2005). "Practical Performance Model for Bar Buckling". *Journal of Structural Engineering*, **131**(7): 1060–1070.

16 Priestley MJN, Seible F and Calvi G (1996). *"Seismic Design and Retrofit of Bridges"*. John Wiley and Sons, New York, USA, 686 pp.

17 Priestley MJN, Calvi GM and Kowalsky MJ (2007). *"Displacement Based Seismic Design of Structures"*. IUSS Press, Pavia, Italy, 721 pp.

18 Peruš I, Poljanˇsek K and Fajfar P (2006). "Flexural deformation capacity of rectangular RC columns determined by the CAE method". *Earthquake Engineering and Structural Dynamics*, **35**(12): 1453–1470.

19 Peruš I and Fajfar P (2007). "Prediction of the force–drift envelope for RC columns in flexure by the CAE method". *Earthquake Engineering and Structural Dynamics*, **36**(15): 2345–2363.

20 Mander JB, Priestley MJN and Park R (1988). "Theoretical Stress Strain Model for Confined Concrete". *Journal of Structural Engineering*, **114**(8): 1804–1826.

21 NTC2008, Ministero delle Infrastrutture e dei Trasporti (2008). *"DM 14 gennaio 2008 in materia di "norme tecniche per le costruzioni". Gazzetta ufficiale n.29 del 4*

febbraio 2008, Supplemento ordinario n.30". Istituto Poligrafico e Zecca dello stato.

22 NZSEE/MBIE (2017). *"The Seismic Assessment of Existing Buildings Technical Guidelines for Engineering Assessments"*. Final draft 1 July 2017, New Zealand.

23 Loporcaro G (2017). *"A Least Invasive Method to Estimate the Residual Strain Capacity in Earthquake-damaged Buildings"*. PhD Dissertation, University of Canterbury, Christchurch, New Zealand, 250 pp.

24 Sadowski AJ, Rotter JM, Stafford PJ, Reinke T and Ummenhofer T (2017). "On the gradient of the yield plateau in structural carbon steels". *Journal of Constructional Steel Research*, **130**: 120-130.

25 King DJ, Priestley MJN and Park R (1986). *"Computer Programs for Concrete Column Design"*. Research Report 86/12, Department of Civil Engineering, University of Canterbury, Christchurch, New Zealand.

26 Priestley MJN and Park R (1987). "Strength and ductility of concrete bridge columns under seismic loading". *ACI Structural Journal*, **84**(1): 61–76.

27 Computer and Structures (2016). *"SAP2000 v18. Structural Analysis Program, Manual"*. Berkeley, California, USA.

LIST OF SYMBOLS

- a_i i[th] coefficient of the characteristic polynomials
- A_{sp} cross-sectional area of one stirrup
- c clear cover of the cross-section
- CF ultimate curvature correction factor
- D diameter of the cross-section
- δ displacement at the tip of the pier
- d_h diameter of one stirrup
- d_l diameter of one longitudinal bar
- ε_c concrete strain
- ε_{ct} concrete strain @ tensile strength
- ε_{sp} concrete spalling strain
- E_c concrete elastic modulus
- E_h transverse steel elastic modulus
- E_s longitudinal steel elastic modulus
- Err error for a single entry of the test series
- Err_{glob} global error of one polynomial (related to the test series)
- F force
- f_c unconfined concrete cylinder compressive strength
- f_{ct} concrete tensile strength (flexure)
- f_t concrete tensile strength (pure tension)
- f_{yh} transverse steel yield stress
- f_{ys} longitudinal steel yield stress
- φ curvature
- φ_Y yield curvature
- χ dimensionless curvature
- χ_{char} curvature for one characteristic point
- $\chi_u(f_c)$ dimensionless ultimate curvature for a given value of f_c
- $\chi_u(31.83)$ dimensionless ultimate curvature for $f_c = 31.83MPa$
- L length of the pier
- L_p equivalent plastic hinge length
- M moment
- m dimensionless moment
- m_{char} moment for one characteristic point
- n_l number of longitudinal bars in the cross-section
- N axial load
- n.a. neutral axis depth
- R radius of the cross-section
- ρ_{sp} volumetric ratio of transverse reinforcement
- s spacing of the stirrups
- υ axial load ratio
- ω mechanical ratio of longitudinal reinforcement

APPENDIX A: DETAILED RESULTS

Table 5: Coefficients of the polynomials: characteristics curvatures.

	χ_{CR}	χ_{Yc}	χ_Y	χ_P	χ_N	χ_{SP}	χ_U
a_0	0.000141687	0.0070035	0.0014652	0.013347	0.009525018	0.014913	0.030808
a_1	0.001179796	-0.025165	0.0041811	-0.054825	-0.016328061	-0.046539	-0.11685
a_2	9.51055E-05	-0.011074	0.00051892	-0.030016	-0.003856943	-0.020517	-0.073578
a_3	0	0	0	1.220752	0	0.010199	5.6901
a_4	0.000641769	0.035666	-0.0133308	0.083624	0.008869441	0.061621	0.15133
a_5	-0.000996454	0.033249	0	0.085899	0.007162256	0.058635	0.19562
a_6	0	0.0072763	-0.00027668	0.019272	0	0.012705	0.051627
a_7	0	0	0	-2.225166	0	0	-6.0449
a_8	0	0	0	0	0	0	-5.1263
a_9	0	-0.017657	0.0087833	-0.0442	0	-0.028807	-0.062491
a_{10}	0	-0.020321	0.00045295	-0.051413	0	-0.034787	-0.11249
a_{11}	0	-0.013063	0	-0.033684	0	-0.022416	-0.08808
a12	0	0	0	1.5519	0	0	1.7707
a13	0	0	0	0.95216	0	0	4.2011
a14	0	0	0	-0.68209	0	0	1.3887

Table 6: Coefficients of the polynomials: characteristics moments.

	m_{CR}	m_{Yc}	m_Y	m_P	m_N	m_{SP}	m_U
a_0	0.039104	0.030715	0.010733	0.054625	0.033077	0.05462	0.008101
a_1	0.24991	0.76049	0.90246	0.52452	0.62906	0.52452	0.691763
a_2	0.019069	0.56557	0.46595	0.59541	0.66	0.59541	0.79591
a_3	0	0.69419	0.25179	-3.2	-0.02506	-3.19999	2.8189
a_4	-0.1041	-1.1359	-1.4939	-0.55922	-0.60654	-0.55922	-0.77233
a_5	0.13464	-0.91382	-0.49555	-0.17954	-0.20421	-0.17953	-0.50387
a_6	0	0	0	-0.02893	-0.034895	-0.02893	-0.18153
a_7	0	-2.8708	0	18.285	6.0638	18.2849	0
a_8	0	-2.3298	0	-1.68543	-1.3176	8.39364	0
a_9	0	0.31306	0.58997	0	0	0	-0.047563
a_{10}	0	0.80451	0.42036	0	0	0	0.50502
a_{11}	0	0	0	0	0	0	0.1109
a_{12}	0	3.3991	0	0	0	0	21.238
a_{13}	0	1.3589	0	0	0	0	-11.155
a_{14}	0	0	0	0	0	0	6.6317
a_{15}	0	0	0	0	0	0	-40.959

Table 7: Test series RC sections, geometric and mechanical properties.

D (m)	c (m)	n_l (-)	d_l (mm)	d_h (-)	s (mm)	f_c (MPa)	f_{ys} (MPa)	N (MN)	ν (-)	ω (-)	ρ_{sp} (-)
1.2	0.06	18	26	14	60	30	380	23	0.678	0.107	0.010
1.4	0.06	17	26	12	70	45	350	31	0.448	0.046	0.005
1.5	0.06	15	32	14	70	26	380	12	0.261	0.100	0.006
2.1	0.04	20	32	16	40	33	390	18	0.158	0.055	0.010
2.5	0.04	23	20	16	50	42	500	75	0.364	0.018	0.007
1.7	0.04	25	20	12	50	37	400	53	0.631	0.037	0.006
1.6	0.07	19	26	14	50	48	360	70	0.726	0.038	0.008
2.0	0.07	19	20	12	45	24	300	36	0.478	0.024	0.005
2.3	0.07	25	18	16	40	29	350	66	0.548	0.018	0.009
1.9	0.05	23	26	14	50	32	440	40	0.441	0.059	0.007

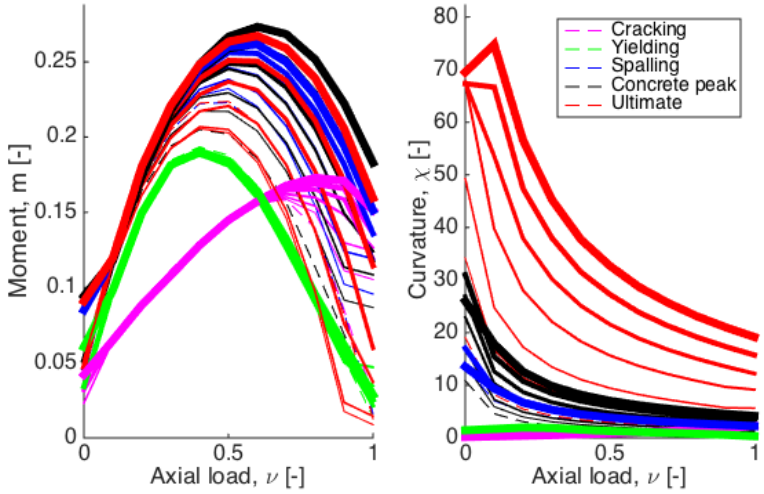

Figure 13: Trend of characteristic moments and curvatures for $\omega = 0.05$ and the full range of ρ_{sp}.

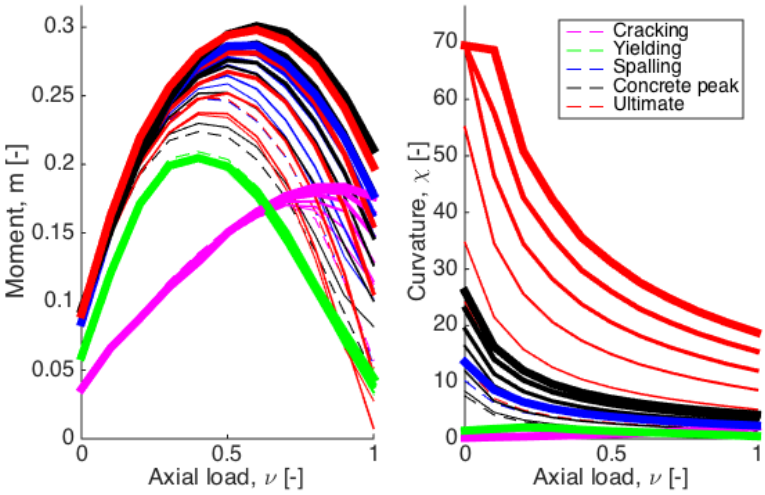

Figure 14: Trend of characteristic moments and curvatures for $\omega = 0.1$ and the full range of ρ_{sp}.

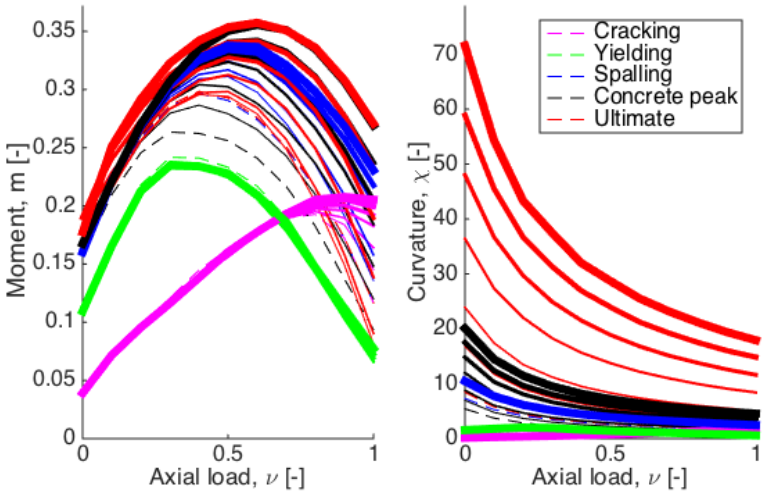

Figure 15: Trend of characteristic moments and curvatures for $\omega = 0.2$ and the full range of ρ_{sp}.

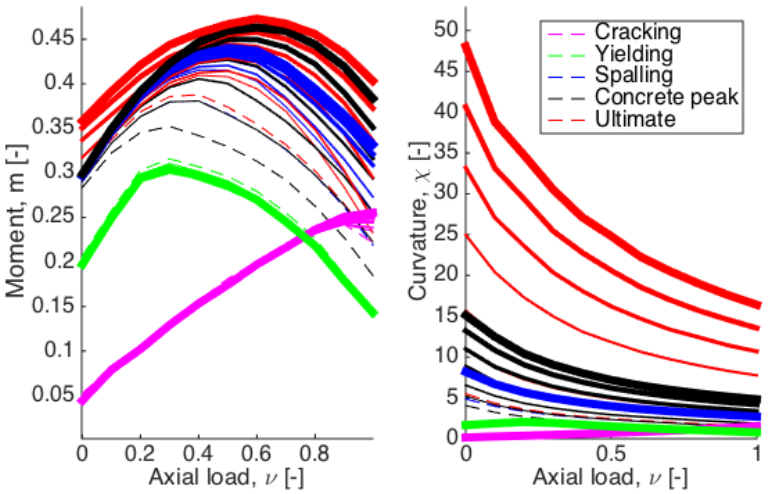

Figure 16: Trend of characteristic moments and curvatures for $\omega = 0.4$ and the full range of ρ_{sp}.

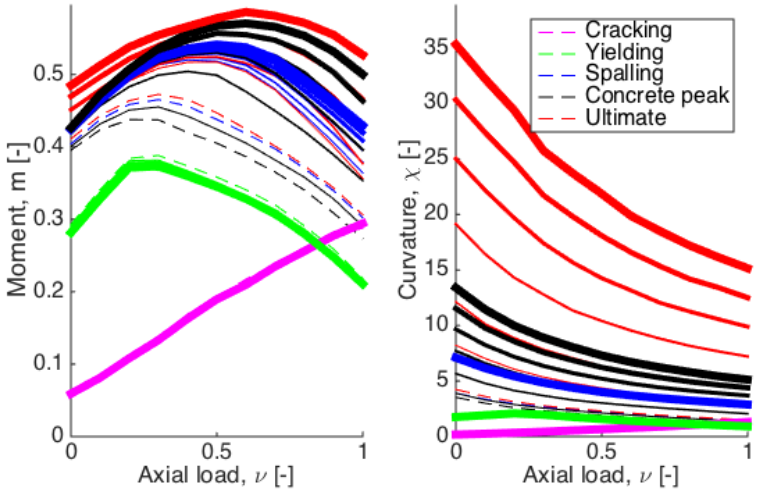

Figure 17: Trend of characteristic moments and curvatures for $\omega = 0.6$ and the full range of ρ_{sp}.

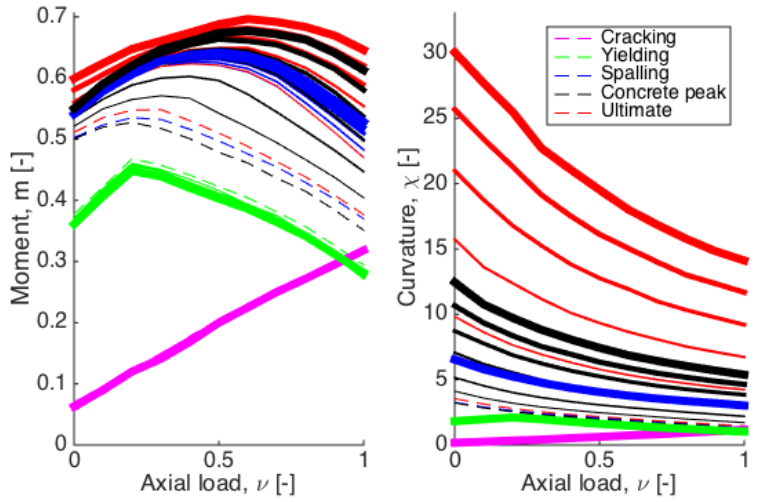

Figure 18: Trend of characteristic moments and curvatures for $\omega = 0.8$ and the full range of ρ_{sp}.